Cholinergic Switching Within Neocortical Inhibitory Networks

Zixiu Xiang, John R. Huguenard, David A. Prince*

Differential actions of acetylcholine on the excitability of two subtypes of interneurons in layer V of the rat visual cortex were examined. Acetylcholine excited low-threshold spike (LTS) cells through nicotinic receptors, whereas it elicited hyperpolarization in fast spiking (FS) cells through muscarinic receptors. Axons of LTS cells were mainly distributed vertically to upper layers, and those of FS cells were primarily confined to layer V. Thus, cortical cholinergic activation may reduce some forms of intralaminar inhibition, promote intracolumnar inhibition, and change the direction of information flow within cortical circuits.

The functional relations between inhibitory and excitatory networks in the neocortex and the modulation of cortical network dynamics by neurotransmitters and peptides (*1*) are important to our understanding of the physiological basis of complex cortical information processing. Different neurotransmitters interact with a variety of receptors whose activation can produce different effects on the excitability of a diverse group of cortical neurons. Predictions of how activation of a given ascending transmitter system affects the flow of information in cortical circuits require integration of data regarding its mode of action at different receptors located on specific subgroups of neurons, which in turn have particular postsynaptic actions and connections in the cortical circuit. Cholinergic activation of subsets of cortical interneurons containing the inhibitory neurotransmitter γ-aminobutyric acid (GABA) provides a case in point.

Cholinergic systems are implicated in several important brain functions, including cortical arousal, sleep-wake cycles, visual information processing, learning, memory, and other cognitive functions (*2*). The dementia of Alzheimer's disease and Parkinson's disease has also been associated, at least in part, with loss of cortical cholinergic innervation (*3*). Detailed information about the effects of cholinergic innervation on the operation of cortical circuits is needed to understand the cellular mechanisms underlying these behavioral and cognitive effects. Neurons in the cerebral cortex have nicotinic as well as muscarinic cholinergic receptors and receive rich cholinergic afferents that arise mainly from groups of neurons located in the basal forebrain, terminate very densely in layer V, and make synapses onto pyramidal cells as well as interneurons (*4*). Neocortical GABA-containing interneurons are highly variable in morphology, spike-firing properties, and immunocytochemical reactivity (*5*–*7*). In layer V, there are several subtypes of electrophysiologically distinct interneurons, with low-threshold spike (LTS) and fast spiking (FS) cells being the most common (*8*). Different interneuronal types have distinct intracortical innervation patterns; for example, the axons of FS interneurons in layer V tend to be distributed more horizontally (intralaminar), whereas LTS cells have more vertical (intracolumnar) axonal arborizations (*7*, *8*). Cholinergic input might thus preferentially affect the behavior of particular subtypes of inhibitory interneurons through different receptors. We tested this hypothesis by examining acetylcholine (ACh) actions on LTS and FS cells.

Interneurons were visualized and recorded in brain slices from rat visual cortex, with whole-cell recording techniques (*9*). ACh was locally applied through a "puffer" pipette, and neuronal responses were recorded and analyzed (*10*). Biocytin was included in the patch electrode recording solution so that cell morphology and axonal arborizations could be subsequently reconstructed (*11*).

Layer V LTS cells displayed characteristic low-threshold spikes that could be elicited by a small depolarizing current pulse from a hyperpolarized membrane potential (−80 mV) (Fig. 1A, left). An initial spike burst followed by a train of spikes could be elicited when a larger depolarizing current step was applied (Fig. 1A, left) (*8*, *12*). FS cells in layer V exhibited distinctly different spike-firing properties, such that superthreshold depolarizing current pulses elicited trains of spikes with little frequency adaptation (Fig. 1A, right) (*8*, *12*, *13*). Twenty-one interneurons were characterized as LTS cells and filled with biocytin, of which five had well-stained soma, dendrites, and axonal arbors. Four of eighteen biocytin-labeled FS interneurons were fairly completely filled. We reconstructed the morphology of these nine cells using a camera lucida. The axonal arborizations of LTS cells tended to be distributed vertically to upper layers (Fig. 1B, left), whereas axonal arbors of FS cells tended to be horizontally distributed and mainly confined to layer V (Fig. 1B, right) (*8*). Laminar analysis of axonal distribution revealed that the total length of axonal arbors in layer V was significantly greater in FS cells than in LTS cells and that LTS cells had more axonal arbors in upper layers than FS cells (Fig. 1C).

Local application of ACh evoked different

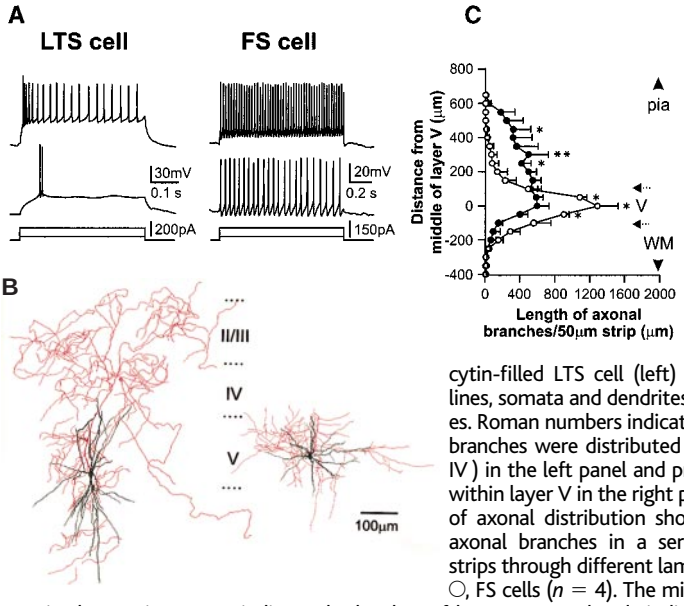

Fig. 1. Electrophysiological and morphological characterization of LTS and FS cells in layer V of visual cortex. (**A**) Current clamp recordings from an LTS cell at membrane potential of −80 mV (left) and an FS cell at −63 mV (right) during injection of depolarizing current pulses of two intensities. (**B**) Camera lucida drawings of the biocytin-filled LTS cell (left) and FS cell (right). Black lines, somata and dendrites; red lines, axonal branches. Roman numbers indicate cortical laminae. Axonal branches were distributed to upper layers (II/III and IV) in the left panel and predominantly horizontally within layer V in the right panel. (**C**) Laminar analysis of axonal distribution showing the total length of axonal branches in a series of horizontal 50-μm strips through different laminae. ●, LTS cells ($n = 5$); ○, FS cells ($n = 4$). The middle of layer V was set as zero in the *y* axis. Arrows indicate the borders of layer V. Arrowheads indicate the directions of pial surface (pia) and white matter (WM). *, $P < 0.05$; **, $P < 0.005$.

Department of Neurology and Neurological Sciences, Stanford University Medical Center, Stanford, CA 94305, USA.

*To whom correspondence should be addressed. E-mail: daprince@leland.Stanford.edu

responses in the two interneuronal subtypes. ACh elicited depolarizing responses in LTS cells ($n = 10$) (Fig. 2A, middle). Depolarizations were sometimes large enough to bring the membrane potential to the spike threshold and cause a quiescent cell to fire action potentials (Fig. 2A, middle). These actions were blocked by the nicotinic receptor antagonist, hexamethonium ($n = 5$) (Fig. 2A, bottom). In contrast, ACh elicited membrane hyperpolarization in all FS neurons that responded (eight of nine) (Fig. 2B, middle). Hyperpolarizations were blocked by scopolamine (5 mM, local application), a muscarinic receptor antagonist, in four of four FS interneurons tested (Fig. 2B, bottom). These differential actions of ACh on LTS versus FS interneurons persisted after perfusion of various solutions that blocked synaptic transmission (Fig. 2, C and D) (*14*). Thus, ACh acted directly on the interneuronal postsynaptic cholinergic receptors.

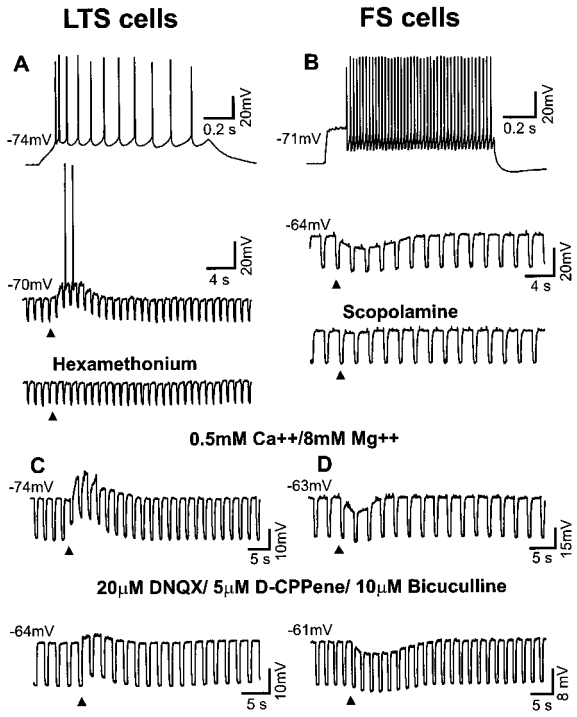

Fig. 2. Typical ACh actions on LTS (**A**) and FS (**B**) cells. (A and B, top) Current clamp recording from an LTS cell (A) and an FS cell (B) in layer V during injection of a depolarizing current pulse, illustrating their spike-firing properties. (A) Local application of ACh (5 mM at 40 kPa for 40 ms) depolarized the membrane potential of the LTS cell (middle). This effect was antagonized by hexamethonium, a nicotinic receptor antagonist (bottom). Arrowheads indicate the time at which ACh was applied. (B) Application of ACh (5 mM at 35 kPa for 80 ms) hyperpolarized the membrane potential of the FS cell (middle), and this action was blocked by a muscarinic receptor antagonist, scopolamine (bottom). Downward fast deflections in middle and bottom panels of (A) and (B): voltage responses to hyperpolarizing current pulses [50 pA for 200 ms at 1 Hz in (A) and 100 pA for 640 ms at 0.5 Hz in (B)]. (**C**) Depolarizing actions of ACh on LTS cells persisted in low-Ca^{++} and high-Mg^{++} perfusate (top) or in the presence of iontropic glutamatergic receptor antagonists, DNQX and D-CPPene, and a $GABA_A$ receptor antagonist, bicuculline (bottom). (**D**) Hyperpolarizing actions of ACh on FS cells remained in low-Ca^{++} and high-Mg^{++} perfusate (top) or in the presence of the glutamatergic receptor antagonists and the $GABA_A$ receptor antagonist (bottom). Arrowheads indicate the time of ACh application. Downward fast deflections: voltage responses to hyperpolarizing current pulses (100 pA for 640 ms at 0.5 Hz). The four panels in (C) and (D) were from four different cells.

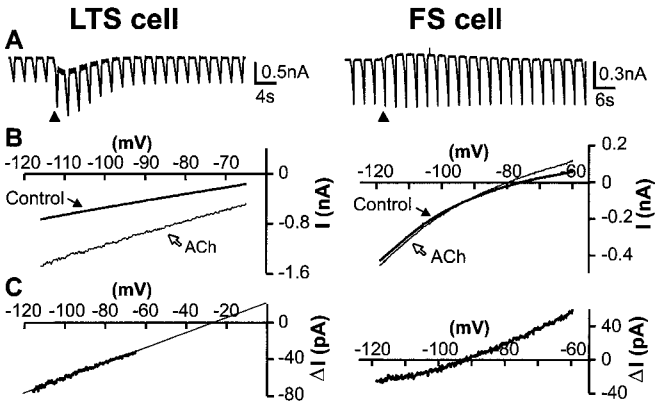

Fig. 3. ACh application elicited an inward current in LTS cells and an outward current in FS cells, both of which were associated with an increase in conductance but with different reversal potentials. (**A**) Voltage clamp recordings from an LTS cell in response to voltage ramps from −65 to −115 mV (left) and from an FS cell with voltage ramps from −60 to −120 mV (right). Local application of ACh induced an inward current in the LTS cell (left) and an outward current in the FS cell (right). The rapid downward deflections are current responses to voltage ramps. Arrowheads indicate the time of ACh application with a pressure pulse (left, 200 ms and 35 kPa; right, 100 ms and 25 kPa). E_{rev} is about −26.6 mV for the LTS cell and −92.1 mV for the FS cell. (**B**) Current versus voltage plots of the LTS cell (left) and FS cell (right) during the hyperpolarizing voltage ramps in control and after ACh application as indicated. Each trace is the mean of 2 to 10 sweeps. (**C**) Subtraction of the two current responses, control and ACh, in (B) ($\Delta I = I_{ACh} - I_{control}$).

To investigate possible ionic mechanisms underlying the differential effects of ACh on LTS and FS cells, we obtained recordings under voltage clamp during application of voltage ramp commands. ACh induced a slow inward current in LTS cells that was associated with an increase in membrane conductance, as indicated by increases in the amplitude of brief downward deflections in response to voltage ramp commands (Fig. 3A, left). In contrast, application of ACh elicited a slow outward current in FS cells that was also accompanied by an increase in membrane conductance (Fig. 3A, right). The reversal potential (E_{rev}) for ACh-induced conductance changes in FS interneurons was −96.1 ± 5.0 mV ($n = 6$), close to the calculated potassium equilibrium potential of −100 mV. The E_{rev} potentials for the nicotinic action on LTS had a mean value of −23.1 ± 7.9 mV ($n = 5$).

Axons of FS cells project primarily to perisomatic areas of layer V pyramidal neurons, and LTS cells have more axonal arbors than FS cells in distal dendritic regions (Fig. 1) (*8*). Consistent with these anatomical observations and the expected electrotonic attenuation of more distal synaptic events (*15*), inhibitory currents generated in pyramidal cells by LTS cells tended to be smaller and have slower rise times than those originating in FS cells (*16*). On the basis of the differential effects of ACh on excitability of LTS cells compared with FS cells, cholinergic excitation should alter the basic aspects of inhibition in layer V pyramidal cells. ACh would increase the frequency of slow, small-amplitude spontaneous inhibitory postsynaptic currents (sIPSCs) in the pyramidal cells by exciting LTS cells and decrease the frequency of fast, larger amplitude events by inhibiting FS cells (*17*). In six of seven recordings from layer V pyramidal neurons, local "puff" application of ACh caused the expected slowing of rise times and attenuation of amplitude of sIPSCs (for example, Fig. 4, A to D). In these six neurons, sIPSC rise time was 0.85 ± 0.02 ms in control, compared with 1.20 ± 0.03 ms in ACh ($P < 0.0001$) and 0.89 ± 0.02 ms after washout ($P > 0.3$, compared with control). Peak amplitude decreased from 39.6 ± 1.1 pA in control to 31.6 ± 0.7 pA ($P < 0.0001$) during ACh exposure and returned to the control level of 40.0 ± 1.1 pA ($P > 0.5$, washout compared with control) (*18*). ACh application did not alter miniature sIPSCs recorded in the presence of TTX (Fig. 4, E and F), suggesting that the effects on sIPSCs in our experiment were due to the direct action on interneuronal excitability, rather than modulation of either presynaptic GABA release machinery or

postsynaptic $GABA_A$ receptors.

Cortical layer V interneurons are diverse not only in their electrophysiological firing properties and axonal arborizations but also in their responsiveness to ACh. Nicotinic receptor-mediated cholinergic excitation of LTS cells was probably mediated by an increase in a mixed cation conductance, similar to that found during nicotinic responses in neurons of other brain regions (*19*–*21*). In contrast, the muscarinic inhibition of FS interneurons appeared to be mediated by an increase in a potassium conductance, similar to that reported during muscarinic hyperpolarization of other GABA-containing neurons (*20*–*22*). Cholinergic excitation of cortical interneurons has been attributed predominantly to activation of muscarinic receptors (*23*–*26*). However, nicotinic excitation of GABA-containing interneurons may also contribute to cortical cholinergic inhibition (*23*, *27*). In contrast to our results, bath application of muscarine is reported to have no effects on FS cells in rat frontal cortex (*25*). This discrepancy could be due to different drug application methods (puff versus bath) or to varieties in cholinergic responsiveness of interneurons in visual versus frontal cortex.

We have demonstrated a selective cortical muscarinic disinhibition; that is, ACh hyperpolarizes a specific type of inhibitory interneuron, FS cells in layer V, resulting in disinhibition of their pyramidal cell targets. Layer V FS interneurons form functional synapses on layer V pyramidal cells (*6*, *16*). Activation of the cortical cholinergic system could thus reduce at least some forms of intralaminar inhibition and, together with direct muscarinic depolarization of layer V pyramidal cells (*23*, *24*), increase pyramid-pyramid recurrent excitation and enhance the intralaminar transfer of information between the cortical columns. Under pathophysiological conditions, a consequence of these actions might be to decrease "surround" inhibition (*28*) and increase the lateral spread of epileptiform discharge. By contrast, nicotinic excitation of LTS cells whose axonal arbors are distributed to upper layers (layers II/III and even I) (Fig. 1) (*8*) would promote intracolumnar inhibition and enhance the inhibitory control of specific excitatory synaptic inputs to the pyramidal cells. Differential modulation of subgroups of inhibitory interneurons by ascending cholinergic or other neurotransmitter systems thus provides a substrate for fine control of information flow in cortical networks.

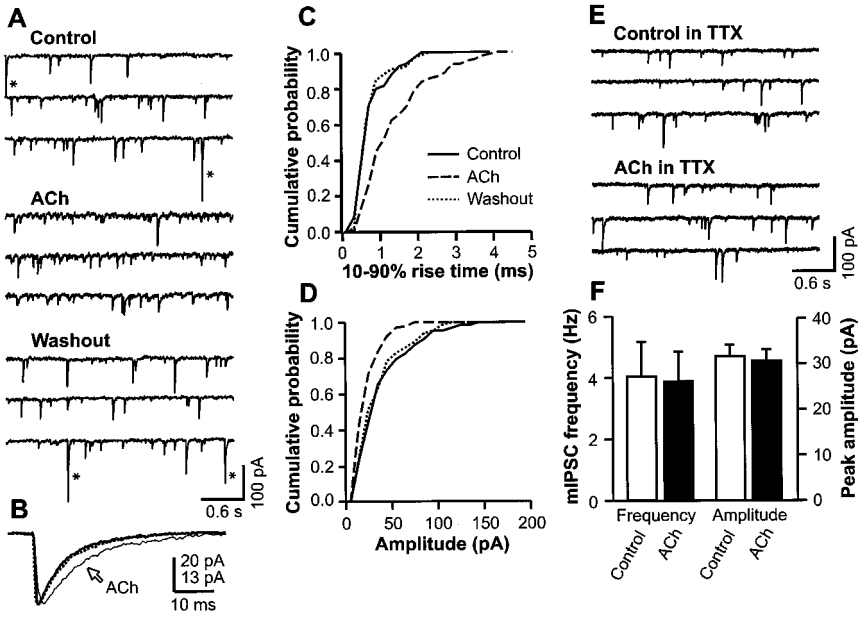

Fig. 4. Effects of local application of ACh on sIPSCs in layer V pyramidal cell. (**A**) sIPSCs recorded at a holding potential of −70 mV in control, after a puff application of ACh (30 ms at 35 kPa) and washout as indicated. Large-amplitude events (*) in control and washout were absent after ACh application, whereas small events were prominent. (**B**) Average traces of consecutive, nonoverlapped sIPSCs (45 to 80 events for each trace) in control (thick trace), during ACh exposure (thin trace), and after washout (dotted trace). Traces were scaled to the same peak amplitude. The calibration is 20 pA for control and washout and 13 pA for ACh. (**C**) Cumulative probability distribution of 10 to 90% sIPSC rise times for 15-s epochs in control (64 events), ACh (103 events), and washout (65 events). Mean sIPSC rise time was 0.81 ± 0.05 ms in control, compared with 1.44 ± 0.09 ms in ACh ($P < 0.0001$, K-S statistics) and 0.79 ± 0.05 ms after washout ($P > 0.5$, compared with control). (**D**) Cumulative probability distribution of sIPSC peak amplitude during the same epochs as in (C). Mean peak amplitude was 40.9 ± 3.7 pA in control, compared with 26.1 ± 1.4 pA during exposure to ACh ($P < 0.0001$) and 39.2 ± 3.2 pA after washout ($P > 0.5$, compared with control). (**E**) Miniature sIPSCs (mIPSCs) recorded in the presence of 1 μM TTX from the same cell as in (A) before and after a similar ACh application as in (A). (**F**) Bar graph summarizing mIPSC frequency and peak amplitude before and after ACh application (15-s epoch each, $n = 5$).

References and Notes

1. M. E. Hasselmo, *Behav. Brain Res.* **67**, 1 (1995).
2. D. J. Stewart, D. F. MacFabe, L. W. Leung, *Brain Res.* **358**, 404 (1985); J. C. Szerb, *J. Physiol.* **192**, 329 (1967); D. A. McCormick and T. Bal, *Annu. Rev. Neurosci.* **20**, 185 (1997); T. G. Aigner and M. Mishkin, *Behav. Neural Biol.* **45**, 81 (1986); R. T. Bartus, R. L. Dean, B. Beer, A. S. Lippa, *Science* **217**, 408 (1982); W. G. Sannita, in *Perspective of Event-Related Potentials Research*, G. Karmos *et al.*, Eds. (Elsevier, Amsterdam, 1995), pp. 156–160; M. M. Mesulam, in *Psychopharmacology: The Fourth Generation of Progress*, F. E. Bloom and D. J. Kupfer, Eds. (Raven, New York, 1995), pp. 135–146.
3. J. T. Coyle, D. L. Price, M. R. DeLong, *Science* **219**, 1184 (1983); P. Davies and A. J. Maloney, *Lancet* **ii**, 1403 (1976); M. Ruberg, A. Ploska, F. Javoy-Agid, Y. Agid, *Brain Res.* **232**, 129 (1982).
4. F. Eckenstein and H. Thoenen, *Neurosci. Lett.* **36**, 211 (1983); C. R. Houser, G. D. Crawford, R. P. Barber, P. M. Salvaterra, J. E. Vaughn, *Brain Res.* **266**, 97 (1983); C. R. Houser, G. D. Crawford, P. M. Salvaterra, J. E. Vaughn, *J. Comp. Neurol.* **234**, 17 (1985); C. B. Saper, *ibid.* **222**, 313 (1984); C. C. Shute and P. R. Lewis, *Brain* **90**, 497 (1967); B. H. Wainer *et al.*, *Brain Res.* **308**, 69 (1984); C. Beaulieu and P. Somogyi, *J. Comp. Neurol.* **304**, 666 (1991).
5. Y. Kawaguchi, C. J. Wilson, S. J. Augood, P. C. Emson, *Trends. Neurosci.* **18**, 527 (1995); C. R. Houser, S. H. Hendry, E. G. Jones, J. E. Vaughn, *J. Neurocytol.* **12**, 617 (1983); P. Somogyi *et al.*, *J. Neurosci.* **4**, 2590 (1984); S. H. Hendry *et al.*, *Exp. Brain Res.* **76**, 467 (1989).
6. A. M. Thomson, D. C. West, J. Hahn, J. Deuchars, *J. Physiol.* **496**, 81 (1996).
7. B. E. Jones and S. H. Hendry, in *Cerebral Cortex*, A. Peters and E. G. Jones, Eds. (Plenum, New York, 1984), pp. 309–336.
8. Y. Kawaguchi, *J. Neurophysiol.* **69**, 416 (1993); Y. Kawaguchi and Y. Kubota, *ibid.* **70**, 387 (1993).
9. Methods for slice preparation and whole-cell recordings from visualized neurons have been previously described [Z. Xiang, J. R. Huguenard, D. A. Prince, *J. Physiol.* **506**, 715 (1998)]. In brief, coronal visual cortical slices (350 μm) were cut from brains of young Sprague-Dawley rats (P12-17) with a vibratome. Ice-cold oxygenated (95% O_2 and 5% CO_2) "cutting solution" contained 230 mM sucrose, 2.5 mM KCl, 0.5 mM $CaCl_2$, 10 mM $MgSO_4$, 1.25 mM NaH_2PO_4, 26 mM $NaHCO_3$, and 10 mM D-glucose. Slices were maintained in oxygenated artificial cerebrospinal fluid (ACSF) at 32°C for a half-hour and then at room temperature for at least 1 hour. They were then transferred to the recording chamber, where they were superfused with ACSF containing 126 mM NaCl, 3 mM KCl, 2 mM $CaCl_2$, 2 mM $MgSO_4$, 1.25 mM NaH_2PO_4, 26 mM $NaHCO_3$, and 10 mM D-glucose at a temperature of ~32°C. Whole-cell patch recordings were made from visually identified interneurons in layer V with infrared video microscopy with Nomarski optics and an EPC-7 patch amplifier (LIST). The pipette solution contained 123 mM potassium gluconate, 10 mM KCl, 1 mM $MgCl_2$, 1 mM $CaCl_2$, 10 mM Hepes, 11 mM EGTA, 3 mM adenosine triphosphate (ATP), and 0.2 to 0.4 mM guanosine triphosphate (GTP). pH was adjusted to 7.3 with 1 M KOH and osmolality to 280 to 290 mosm with distilled water. Biocytin (0.3 to 0.4 %) was also included in the pipette solution. The liquid junction potential with this pipette solution was estimated to be about 9 mV, and the membrane potential was corrected accordingly. Patch pipettes had resistances of 3 to 4 Mohm when filled with the above the pipette solution. Series resistance (R_s) typically ranged from 9 to 15 Mohm. Only recordings with <15% change in R_s were included in this study. In voltage clamp experiments, R_s was compensated about 50 to 75 %.
10. About 20 to 50 pl of 5 mM ACh was applied by

pressure pulses (25 to 40 kPa for 25 to 200 ms) through a "puffer" pipette (2 to 4 μm in tip diameter) placed 40 to 60 μm away from the recorded cell. Muscarinic and nicotinic receptor antagonists, scopolamine (5 mM) and hexamethonium (5 mM), were applied in 30 to 50 μl of ACSF directly into the recording chamber while it was perfused with ACSF at the rate of 1.5 ml/min. Effects of these antagonists usually appeared within 1 to 4 min. Other agents such as 6,7-dinitroquinoxoline-2,3-dione (DNQX, 20 μM) and 3-(2-carboxypiperazin-4-yl)-1-propenyl-1-phosphonic acid (D-CPPene, 5 μM), GABA receptor antagonist, and bicuculline (10 μM), as well as tetrodotoxin (TTX, 1 μM), were added to the perfusate and bath applied. To estimate the reversal potential of ACh-induced conductance changes, we plotted the current responses versus ramp voltage in control solution and after drug application and obtained current difference–voltage (ΔI-V) plots by subtracting the control current from ACh current. We estimated the reversal potentials by extrapolating the linear fitting curve to $\Delta I = 0$ or using the crossing points of the ΔI-V curve to the voltage axis at $\Delta I = 0$ (Fig. 3).

11. After the physiological experiments, slices containing biocytin-filled neurons were processed with standard avidin-biotin-peroxidase methods as described elsewhere in detail [K. Horikawa and W. E. Armstrong, *J. Neurosci. Methods* **25**, 1 (1988); G. F. Tseng, I. Parada, D. A. Prince, *ibid.* **37**, 121 (1991)]. Labeled neurons were examined under the light microscope and drawn with a camera lucida, and the axonal arbor representations were exported as bitmap files. Total axonal length per 50-μm horizontal strip was estimated by measuring the integrated bitmap density. Data were then aligned approximately to the middle of the layer V for statistical analysis for which the Mann-Whitney test was used. The results were presented as mean ± SEM.
12. R. C. Foehring, N. M. Lorenzon, P. Herron, C. J. Wilson, *J. Neurophysiol.* **66**, 1825 (1991).
13. D. A. McCormick, B. W. Connors, J. W. Lighthall, D. A. Prince, *ibid.* **54**, 782 (1985).
14. The differential action of ACh on LTS compared with FS cells remained after synaptic transmission was blocked by perfusing the slice with ACSF containing low Ca^{++} (0.5 mM) and high Mg^{++} (8 mM) [$n = 3$ for LTS cells and $n = 3$ for FS cells; Fig. 2, C (top) and D (top)]; glutamatergic receptor antagonists, DNQX (20 μM) and D-CPPene (5 μM), and the $GABA_A$ receptor antagonist, bicuculline (10 μM) [$n = 2$ for LTS cells and $n = 2$ for FS cells; Fig. 2, C (bottom) and D (bottom)]; or 1 μM TTX ($n = 3$ for LTS and $n = 2$ for FS; Z. Xiang, J. R. Huguenard, D. A. Prince, data not shown).
15. A. U. Larkman, G. Major, K. J. Stratford, J. J. Jack, *J. Comp. Neurol.* **323**, 137 (1992); N. Spruston, D. B. Jaffe, D. Johnston, *Trends. Neurosci.* **17**, 161 (1994).
16. Z. Xiang, I. Parada, J. R. Huguenard, D. A. Prince, *Soc. Neurosci. Abstr.* **23**, 359 (1997).
17. In experiments in which effects of ACh on sIPSCs from layer V pyramidal cells were examined, the extracellular KCl was increased to 10 mM to increase the frequency of spike-driven events, and DNQX (20 μM) and D-CPPene (5 μM) were included in perfusate to block the ionotropic glutamatergic synaptic transmission. Pipette solution contained 65 mM KCl, 65 mM potassium gluconate, 1 mM $MgCl_2$, 1 mM $CaCl_2$, 10 mM Hepes, 10 mM EGTA, 3 mM ATP, and 0.2 to 0.4 mM GTP. With this pipette solution, calculated chloride equilibrium potential was −15 mV based on the Nernst equation with activity coefficients for extracellular Cl^- of 0.76 and intracellular Cl^- of 0.80 and taking into account the permeability of gluconate through Cl^- channels [J. L. Barker and N. L. Harrison, *J. Physiol.* **403**, 41 (1988)]. In such a recording condition, sIPSCs were inward currents at a holding potential of −70 mV. ACh were locally applied as described in (*10*). Kolmogorov-Smirnov (K-S) statistics were used to analyze the sIPSC data.
18. In one pyramidal cell, ACh application gave rise to an increase in frequency of large, slow events. This cell showed an increase in sIPSC rise time after ACh application similar to that seen in six other neurons. We speculate that the large-amplitude sIPSCs in this particular case may have reflected an unusually large number of synaptic contacts from one or more LTS cells onto the pyramidal neuron.
19. D. A. McCormick and D. A. Prince, *J. Neurosci.* **7**, 742 (1987); L. J. Reece and P. A. Schwartzkroin, *Brain Res.* **540**, 287 (1991); A. R. McQuiston and D. V. Madison, *Soc. Neurosci. Abstr.* **23**, 2009 (1997); C. J. Frazier *et al.*, *J. Neurosci.* **18**, 1187 (1998); M. Alkondon, E. F. Pereira, C. T. Barbosa, E. X. Albuquerque, *J. Pharmacol. Exp. Ther.* **283**, 1396 (1997).
20. K. H. Lee and D. A. McCormick, *J. Neurophysiol.* **73**, 2123 (1995).
21. A. R. McQuiston and D. V. Madison, *Soc. Neurosci. Abstr.* **22**, 786 (1996).
22. D. A. McCormick and D. A. Prince, *Nature* **319**, 402 (1986); D. A. McCormick and H. C. Pape, *ibid.* **334**, 246 (1988).
23. D. A. McCormick and D. A. Prince, *Proc. Natl. Acad. Sci. U.S.A.* **82**, 6344 (1985).
24. _____, *J. Physiol.* **375**, 169 (1986).
25. Y. Kawaguchi, *J. Neurophysiol.* **78**, 1743 (1997).
26. L. J. Reece and P. A. Schwartzkroin, *Brain Res.* **566**, 115 (1991); T. A. Pitler and B. E. Alger, *J. Physiol.* **450**,127 (1992).
27. J. W. Phillis and D. H. York, *Brain Res.* **10**, 297 (1968); K. Krnjevic, *Physiol. Rev.* **54**, 418 (1974).
28. D. A. Prince and B. J. Wilder, *Arch. Neurol.* **16**, 194 (1967).
29. We thank I. Parada for her excellent assistance during the course of the experiments. The work was supported by NIH grants NS 12151, NS 07280, NS 06477, and NS 10474 from the National Institute of Neurological Disorders and Stroke and the Morris and Pimley research funds.

7 April 1998; accepted 8 July 1998

Neural Crest Specification Regulated by the Helix-Loop-Helix Repressor Id2

Brad J. Martinsen and Marianne Bronner-Fraser*

Vertebrate neural crest cells, derived from the neural folds, generate a variety of tissues, such as cartilage, ganglia, and cranial (intramembranous) bone. The chick homolog of the helix-loop-helix transcriptional regulator Id2 is expressed in cranial but not trunk neural folds and subsequently in some migrating cranial neural crest cells. Ectopic expression of Id2 with recombinant retroviruses converted ectodermal cells to a neural crest fate, demonstrating that proper regulation of Id2 is important for sustaining epidermal traits. In addition, overexpression of Id2 resulted in overgrowth and premature neurogenesis of the dorsal neural tube. These results suggest that Id2 may allocate ectodermal precursors into neural rather than epidermal lineages.

Neural crest cells follow migratory pathways and generate final cell types in accordance with their original rostrocaudal position along the axis (*1*, *2*). Although both cranial and trunk neural crest cells can form melanocytes, glia, sensory neurons, and autonomic neurons (*3*, *4*), only cranial neural crest cells have the ability to form cartilage and bone (*2*, *5*). In screening for transcripts that are selectively expressed in cranial but not trunk neural folds (*6*), we isolated the chick homolog of Id2 (*7*) (Fig. 1, A and B). Id proteins (inhibitors of DNA binding) are negative regulators of basic helix-loop-helix (bHLH) transcription factors (*7–10*) that are involved in developmental processes such as myogenesis (*9*, *11–13*), neurogenesis (*14*, *15*), bone morphogenesis (*16*), lymphopoiesis (*17*), hematopoiesis (*18*), myeloid differentiation (*19*), and cell growth (*20–22*). We show that Id2 directs ectodermal precursor toward neural crest and neurogenic fates.

In situ hybridization revealed *Id2* transcripts in the most dorsal cranial neural fold region of the presumptive brain (Fig. 2, A and B). The caudal border of expression approximately corresponds to the midvagal region (Fig. 2, A and C) at the rhombomere 7/8 boundary and is maintained beyond stage 17. As neural crest cells migrated out of the neural tube, *Id2* was expressed by a subpopulation of migrating cranial neural crest cells at the midbrain level (Fig. 2D). Transverse sections show *Id2* mRNA in recently emigrated neural crest cells as they move toward the branchial arches (Fig. 2E). At later stages, Id2 was expressed in the region of forming cranial ganglia, such as the ciliary and trigeminal ganglia. Within the neural tube, expression became restricted to the alar plate in stage 28 embryos. In addition to expression in cranial neural fold derivatives, *Id2* was expressed in the somites and subsequently in vertebral cartilage.

We explored the functional importance of Id2 in vivo by overexpressing it in the chick embryo using retrovirally mediated gene transfer with RCASBP (B) virus (replication-competent avian leukemia virus LTR splice acceptor Bryan polymerase, subgroup B envelope

B. J. Martinsen, Division of Biology, Beckman Institute 139-74, California Institute of Technology, Pasadena, CA 91125, USA, and Department of Developmental and Cell Biology, University of California, Irvine, CA 92717, USA. M. Bronner-Fraser, Division of Biology, Beckman Institute 139-74, California Institute of Technology, Pasadena, CA 91125, USA.

*To whom correspondence should be addressed. E-mail: mbronner@caltech.edu